2019 Living Planet Symposium 2019 (1719)

Evaluation of dynamical properties of the surface currents and sea surface heights in a coastal region

Eun Ae Lee and Sung Yong Kim†

Department of Mechanical Engineering, Korea Advanced Institute of Science and Technology,
syongkim@kaist.ac.kr†

Mechanical Engineering

KAIST

NRF National Research Foundation of Korea

Abstract

We conduct statistical and spectral analyses on the (1) observations of costal radar-derived surface currents and altimeter-derived geostrophic currents and (2) forward regional circulation model simulations forced with realistic wind stress, tides, and boundary conditions off the Oregon coast in view of the geostrophy and ageostrophy and the balanced and unbalanced motions. Delineation of balanced and unbalanced motions was investigated with the Helmholtz decomposition in the physical and spectral spaces and wave-vortex spectral decomposition. The observed and simulated coastal surface currents do not exhibit the clear decomposition of the balanced motions and unbalanced motions because wave-vortex decomposition may not always work in the coastal regions where multiple sources of dominant variances are available. On the other hand, the stream functions obtained from the Helmholtz physical decomposition can be a proxy of the balanced motions when the variance of vertical currents is weak. The submesoscale ageostrophic currents account for up to 50% of the total variance and are primarily associated with near-inertial currents and internal tides, which can be missing components in the currents retrieved from solely submesoscale SSHs. As the pure SSHs may not constrain the entire submesoscale ageostrophic components, the missing variance in the submesoscale SSH observations is required to be complementary with other high-resolution *in-situ* observations, including HFR-derived surface velocities and surface drifter-derived tracks in a view of constructive data integration to resolve submesoscale currents.

Data

A study domain for numerical simulations using the Regional Ocean Modeling System (ROMS) and MIT general circulation model (MITgcm), ranging from 40.6°N to 50°N and 130°W to the coast (approximately 450 km cross-shore distance; Figure 1a), is divided into four subdomains for detailed investigations (D1, D2, D3, and D4): a zonal (cross-shore) line (D1) at 44.65°N as a cross-shore extension of the NH10 line, two 1° square boxes in the coastal and offshore regions centered over the NH10 line (D2 and D3), and a latitudinal (zonal) band centered over the NH10 line (D4) with a width of 0.25°.

A coastal region in the northeastern Pacific is chosen as the study domain because (1) realistic numerical model simulations and observations of altimetry-derived sea surface height anomalies (SSHAs)

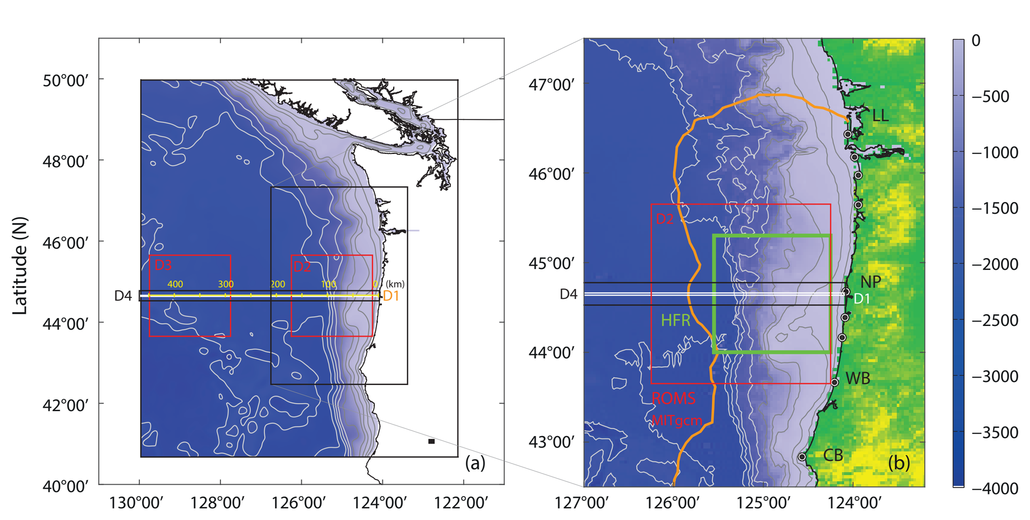

Figure 1: (a) A domain for numerical simulations using ROMS and MITgcm, ranging from 130°W to the coast and between 40.6°N and 50°N for the study of submesoscale coastal surface currents to high-resolution sea surface heights (SSHs) off the coast of Oregon. (b) A close-up of the nearcoast region to overlap the ROMS and MITgcm simulations (a red box; D2) and HFR-derived surface current observations (an orange contour and a green box) where the azimuthally averaged wavenumber-frequency-domain energy spectra are estimated As a reference, major coastal regions are denoted by abbreviated two letter names from south to north: Cape Blanco (CB), Winchester Bay (WB), Newport (NP), and Loomis Lake (LL). The bottom bathymetry in Figures 1a and 1b is contoured at 50 m, 100 m, 250 m, 500 m, 1000 m, 1500 m, 2000 m, 2500 m, and 3000 m.

and geostrophic currents and HFR-derived submesoscale coastal surface currents are available along a relatively simple coastline, and (2) there is a clear separation of the variance between local inertial frequency and two primary tides (K_1 and M_2).

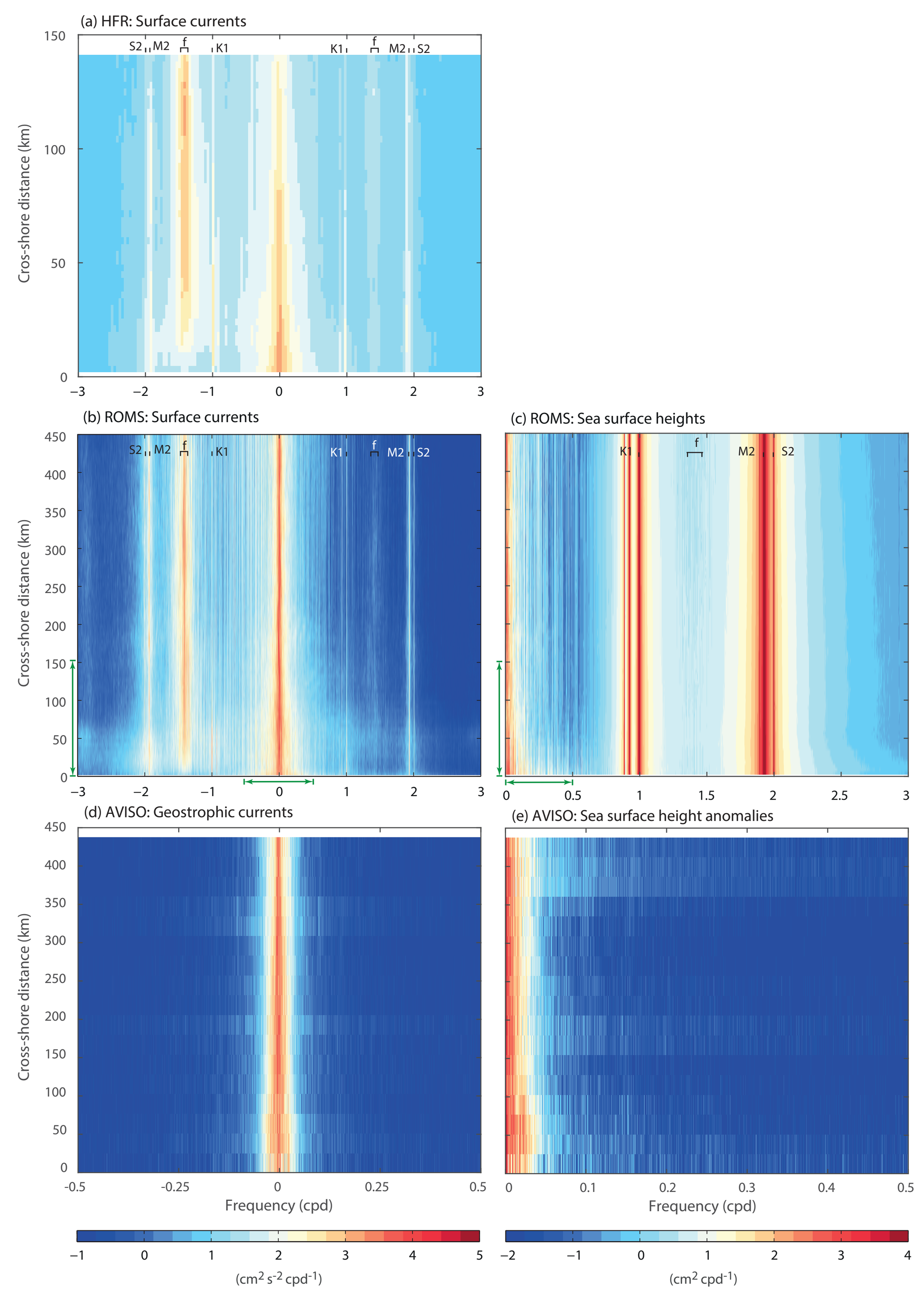

Figure 2: Meridionally averaged rotary energy spectra ($\log_{10}$ scale; $\mathrm{cm^2\,s^{-2}\,cpd^{-1}}$) of the (a) HFR-derived surface currents, (b) ROMS-simulated surface currents, (c) ROMS-simulated SSHs, (d) AVISO geostrophic currents, and (e) AVISO SSHAs in D4. Green arrows on both axes in Figure 2b correspond to the frequency and cross-shore distance in Figure 2a and 2d.

We analyze two different numerical simulation outputs off the Oregon coast: (1) the SSHs and currents with hourly temporal and 2-km horizontal spatial resolutions for a period of approximately one year (August 2008 to August 2009) obtained from forward numerical simulations, which were forced by realistic wind stress and tides using the ROMS under the hydrostatic assumption and (2) the SSHs and currents with hourly temporal and 1/48° (approximately 1.5 km) horizontal spatial resolutions for a period of approximately one year (September 13, 2011 to November 15, 2012) using MITgcm (llc4320) under the non-hydrostatic assumption.

The near-inertial variance in the stream functions (Figure 4f) can be explained by the advection of near-inertial currents as the non-propagating components or non-divergent horizontal near-inertial currents. The near-inertial variance in the azimuthally averaged energy spectra of the HFR-derived and ROMS-simulated surface currents are mostly found in the frequency band lower than where the IGWs under the regional buoyancy frequency and depth exist. However, the unbalanced near-inertial motions can be found in the velocity potential-derived current components (Figures 3b, 3d, and 4e).

Geostrophic and ageostrophic currents

The variances of the geostrophic and ageostrophic currents estimated from spatial derivatives of SSHs are dominant at the length scales longer and shorter than 10 to 20 km (Figure 3a), respectively. However, simple spatial derivatives of the SSHs may not be valid for high-wavenumber and high-frequency bands, as the geostrophic balance is not valid in those wavenumber and frequency bands and the variances of the geostrophic and ageostrophic currents appear to be higher than the variance in the total surface currents (Figure 3b). In the case that a series of the SSH maps obtained from the SWOT mission are available, the spatial derivatives of the SSHs using geostrophic balance and their wavenumber-domain energy spectra can be estimated without their temporal variability because the time interval between individual SSH maps is long (e.g., a few days); therefore, we may not consider them a time series. Thus, the wavenumber-domain energy spectra of the ROMS-simulated and MITgcm-simulated surface currents in Figures 3a and 3c are examples of when the geostrophic currents and internal tides (M_2) are dominant, respectively. The variance in the currents estimated from the geostrophic balance can be higher than the variance of the total currents (Figures 3c and 3d), which serves as a cautionary remark on the analysis of a series of high-resolution SSH maps.

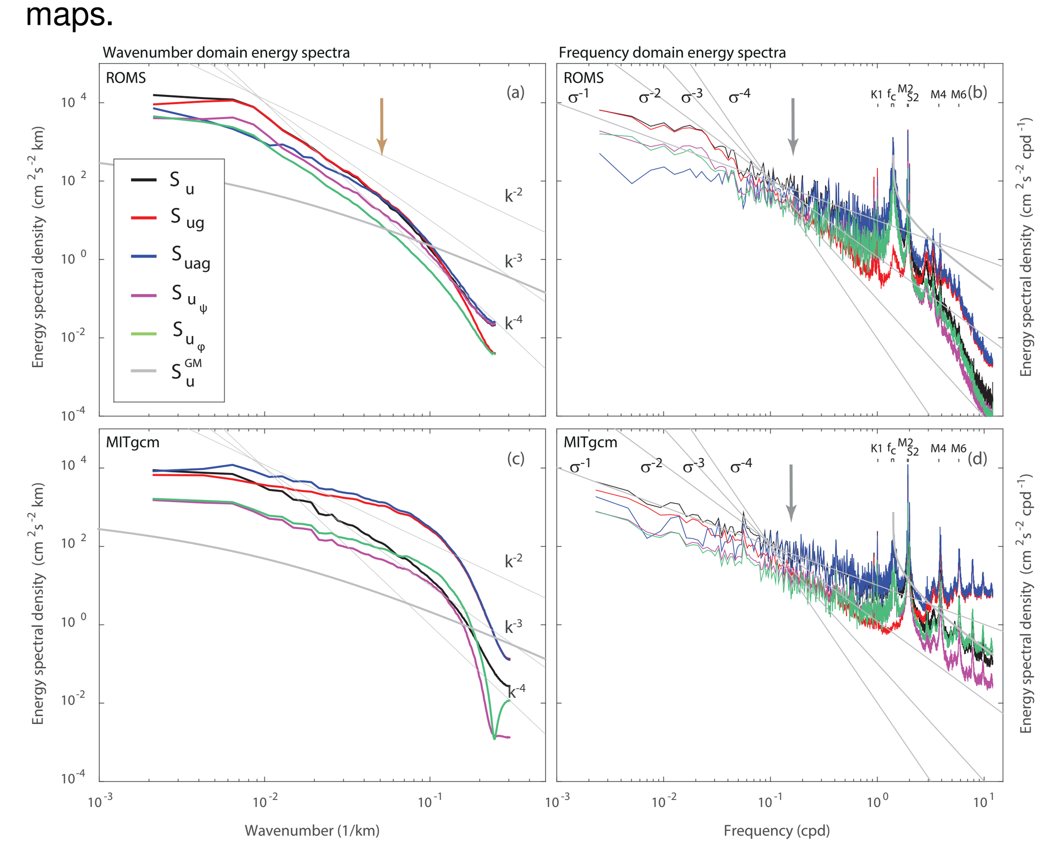

Figure 3: [(a) and (c)] Wavenumber-domain and [(b) and (d)] frequency-domain energy spectra of the currents, sampled on the NH10 line (D1). (a) and (b): Energy spectra of the ROMS-simulated surface currents ($S_{\mathbf{u}}$), geostrophic currents ($S_{\mathbf{u}_g}$), ageostrophic currents ($S_{\mathbf{u}_{ag}}$), surface currents corresponding to the Helmholtz (physical) decomposed stream functions ($S_{\mathbf{u}_\psi}$) and velocity potential ($S_{\mathbf{u}_\phi}$), and the Garrett-Munk (GM) spectrum ($S^{\mathrm{GM}}_{\mathbf{u}}$). (c) and (d): Energy spectra of the MITgcm-simulated surface currents ($S_{\mathbf{u}}$), geostrophic currents ($S_{\mathbf{u}_g}$), ageostrophic currents ($S_{\mathbf{u}_{ag}}$), surface currents corresponding to the Helmholtz (physical) decomposed stream functions ($S_{\mathbf{u}_\psi}$) and velocity potential ($S_{\mathbf{u}_\phi}$), and the Garrett-Munk (GM) spectrum ($S^{\mathrm{GM}}_{\mathbf{u}}$).

Energy partitioning in the wavenumber domain

The total energy [$E(k)$] of ocean surface currents under nonhydrostatic surface waves ($S_w = 0$ if the waves are hydrostatic) is conserved as the sum of the kinetic energy [$E_k(k)$] and potential energy [$E_p(k)$], presented as the wavenumber-domain energy spectra as follows,

$$
\begin{aligned}
E(k) &= E_k(k) + E_p(k), &(1)\\
&= \frac{1}{2}\left[S_u(k) + S_v(k) + S_w(k)\right] + \frac{1}{2}S_b(k), &(2)
\end{aligned}
$$

where

$$
[S_u(k), S_v(k), S_w(k)] = \frac{1}{\Delta k}\left|\frac{1}{M}\sum_{m=1}^{M}\left[u(x_m), v(x_m), w(x_m)\right]e^{-ikx_m}\right|^2, \quad (3)
$$

$$
S_b(k) = \frac{1}{\Delta k}\left|\frac{1}{M}\sum_{m=1}^{M}\frac{b(x_m)}{\mathsf{N}(x_m)}e^{-ikx_m}\right|^2, \quad (4)
$$

and M, S_b, w, ρ_0, g, and b denote the number of evenly spaced sampling (zonal) grid points, buoyancy spectrum normalized by buoyancy frequency (N; s^{-1}), vertical velocity, reference density, gravitational acceleration, and reduced gravity, respectively. The spectrum of internal gravity waves is presented with the GM spectrum.

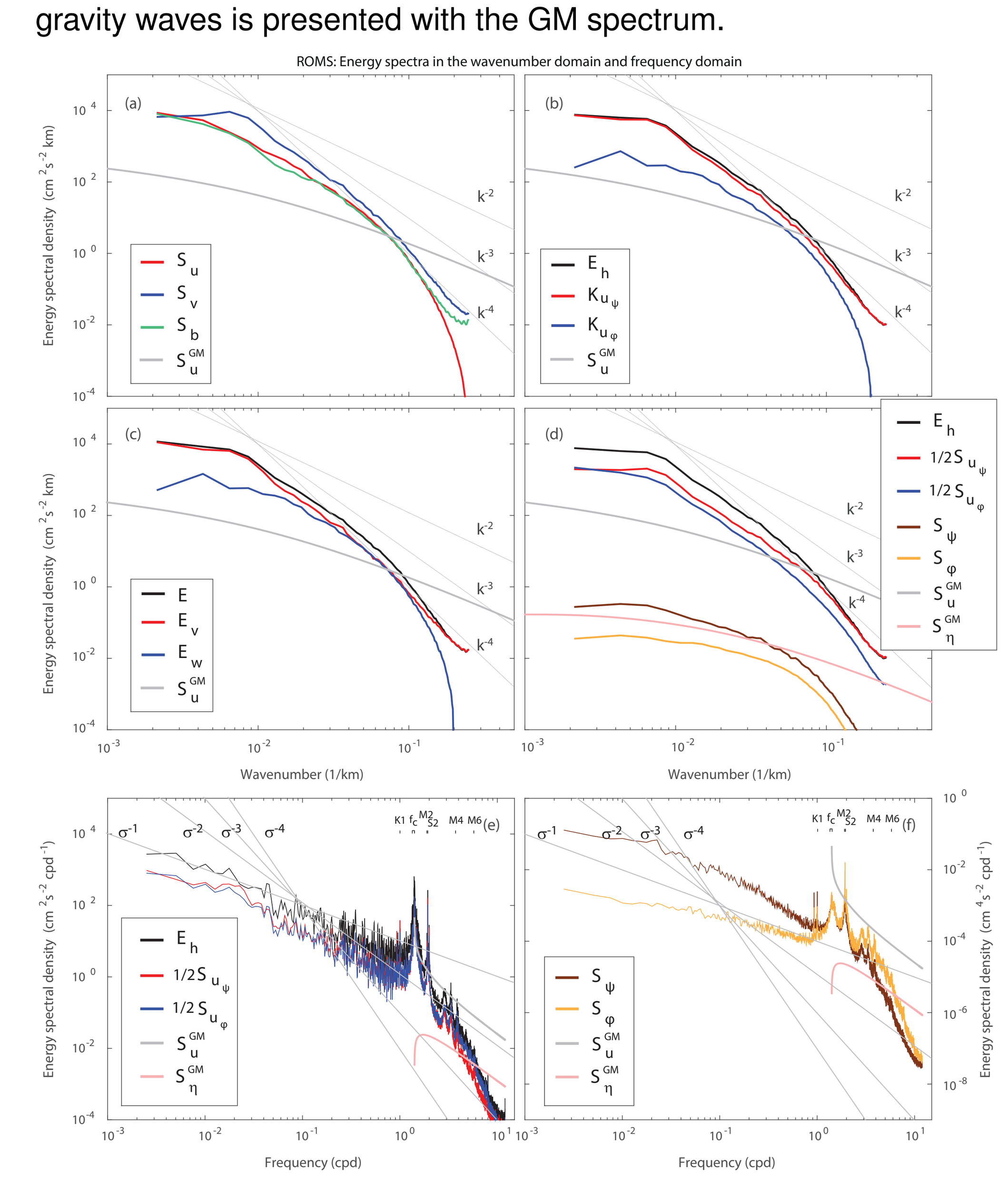

Figure 4: (a) to (d): Wavenumber-domain energy spectra of the ROMS-simulated surface currents on the NH10 line (D1). (a) Energy spectra of the zonal and meridional velocity components (S_u and S_v) and buoyancy (S_b). (b) Energy spectra of the horizontal velocity components (E_h) and horizontal velocity components of the Helmholtz (spectral) decomposed stream function ($K_{\mathbf{u}_\psi}$) and velocity potential ($K_{\mathbf{u}_\phi}$). (c) Energy spectra of total energy (E) and the wave-vortex decomposed balanced motions (E_v) and unbalanced motions (E_w). (d) Energy spectra of the horizontal velocity components (E_h) and the horizontal velocity components of the Helmholtz (spectral) decomposed stream function ($\frac{1}{2}S_{\mathbf{u}_\psi}$) and velocity potential ($\frac{1}{2}S_{\mathbf{u}_\phi}$), and the Helmholtz (physical) decomposed stream function (S_ψ) and velocity potential (S_ϕ) using optimal interpolation. (e) and (f): Frequency-domain energy spectra of the ROMS-simulated horizontal velocity components (E_h) and the horizontal velocity components of the Helmholtz (physical) decomposed stream function ($\frac{1}{2}S_{\mathbf{u}_\psi}$) and velocity potential ($\frac{1}{2}S_{\mathbf{u}_\phi}$), and the Helmholtz (physical) decomposed stream function (S_ψ) and velocity potential (S_ϕ) on the NH10 line (D1).

The kinetic energy [$E_h(k)$] associated with the horizontal velocity components is conserved with the kinetic energy spectra of the currents corresponding to stream functions [$K_{\mathbf{u}_\psi}(k)$; equation 6] and velocity potential [$K_{\mathbf{u}_\phi}(k)$; equation 7] using the Helmholtz spectral decomposition under horizontal anisotropy,

$$
E_h(k) = \frac{1}{2}\left[S_u(k) + S_v(k)\right] = K_{\mathbf{u}_\psi}(k) + K_{\mathbf{u}_\phi}(k), \quad (5)
$$

where

$$
K_{\mathbf{u}_\psi}(k) = \frac{1}{2}S_v(k) + \frac{1}{2k}\int_k^\infty\left[S_v(\kappa) - S_u(\kappa) + \frac{\langle u^2\rangle - \langle v^2\rangle}{\langle uv^\ddagger\rangle}S_{uv}(\kappa)\right]\mathrm{d}\kappa, \quad (6)
$$

$$
K_{\mathbf{u}_\phi}(k) = \frac{1}{2}S_u(k) - \frac{1}{2k}\int_k^\infty\left[S_v(\kappa) - S_u(\kappa) + \frac{\langle u^2\rangle - \langle v^2\rangle}{\langle uv^\ddagger\rangle}S_{uv}(\kappa)\right]\mathrm{d}\kappa, \quad (7)
$$

$$
S_{uv}(k) = \frac{1}{\Delta k}\left|\left(\frac{1}{M}\sum_{m=1}^{M}u(x_m)e^{-ikx_m}\right)\left(\frac{1}{M}\sum_{m=1}^{M}v(x_m)e^{-ikx_m}\right)^\dagger\right|, \quad (8)
$$

and †, ‡, and $\langle\cdot\rangle$ denote the complex conjugate transpose, vector transpose, and expectation of the given variable, respectively. The variance and covariance of the velocity components are implemented with their spatial averages in the wavenumber-domain integration (equations 6 and 7).

In the same way, the total energy is conserved as the sum of the energy spectra of the unbalanced wave components [$E_{\mathbf{w}}(k)$; equation 11] and balanced vortical components [$E_{\mathbf{v}}(k)$; equation 12] using non-hydrostatic linear wave-vortex spectral decomposition under assumptions of isotropy, stationarity, and homogeneity of the currents as follows,

$$
\begin{aligned}
E(k) &= E_{\mathbf{v}}(k) + E_{\mathbf{w}}(k), &(9)\\
&= K_{\mathbf{u}_\psi}(k) + K_{\mathbf{u}_\phi}(k) + \frac{1}{2}\left[S_w(k) + S_b(k)\right], &(10)
\end{aligned}
$$

where

$$
\begin{aligned}
E_{\mathbf{w}}(k) &= 2K_{\mathbf{u}_\phi}(k) + S_w(k), &(11)\\
E_{\mathbf{v}}(k) &= E(k) - E_{\mathbf{w}}(k), &(12)\\
&= K_{\mathbf{u}_\psi}(k) - K_{\mathbf{u}_\phi}(k) + \frac{1}{2}\left[-S_w(k) + S_b(k)\right]. &(13)
\end{aligned}
$$

Summary

We evaluate the dynamical properties of the surface currents and sea surface heights in a coastal region with statistical and spectral analyses of (1) observations of coastal radar-derived surface currents and altimeter-derived geostrophic currents and (2) forward regional circulation model simulations (ROMS and MITgcm) forced with realistic wind stress, tides, and boundary conditions off the Oregon coast in view of the geostrophy and ageostrophy and the balanced and unbalanced motions.

As anomalies from the geostrophic currents, which are the balanced currents between the Coriolis force and pressure gradients caused by the slope of SSHs, ageostrophic currents account for up to 50% of the total variance, which are primarily associated with near-inertial currents and internal tides, which can be missing components in the currents retrieved from solely submesoscale SSHs. As the pure SSHs may not constrain the entire submesoscale ageostrophic components, the missing variance in the submesoscale SSH observations requires to be complemented with other concurrent high-resolution *in-situ* observations, including HFR-derived surface velocities and surface drifter-derived tracks, and data-assimilated techniques to stitch the observations and numerical models together in view of constructive data integration to resolve submesoscale currents.

Acknowledgement

This work is supported by grants through Basic Science Research Program through the National Research Foundation (NRF), Ministry of Education (NRF-2017R1D1A1B03028285), the Disaster and Safety Management Institute, Ministry of Public Safety and Security (KCG-01-2017-05), and the Khalifa University of Science,Technology and Research (KUSTAR)-Korea Advanced Institute of Science and Technology (KAIST) Institute, KAIST (SMP-N11190100), Republic of Korea. Special thanks to P. Michael Kosro and Alexander Kurapov at OSU for surface current data and numerical model outputs.